PCCP

ROYAL SOCIETY OF CHEMISTRY

PAPER

View Article Online
View Journal | View Issue

Cite this: *Phys. Chem. Chem. Phys.*, 2024, **26**, 6127

Types of noncovalent bonds within complexes of thiazole with CF_4 and SiF_4

Steve Scheiner *[a] and Akhtam Amonov [b]

The five-membered heteroaromatic thiazole molecule contains a number of electron-rich regions that could attract an electrophile, namely the N and S lone pairs that lie in the molecular plane, and π-system areas above the plane. The possibility of each of these sites engaging in a tetrel bond (TB) with CF_4 and SiF_4, as well as geometries that encompass a CH···F H-bond, was explored *via* DFT calculations. There are a number of minima that occur in the pairing of thiazole with CF_4 that are very close in energy, but these complexes are weakly bound by less than 2 kcal mol^{-1} and the presence of a true TB is questionable. The inclusion of zero-point vibrational energies alters the energetic ordering, which is further modified when entropic effects are added. The preferred geometry would thus be sensitive to the temperature of an experiment. Replacement of CF_4 by SiF_4 leaves intact most of the configurations, and their tight energetic clustering, the ordering of which is again altered as the temperature rises. But there is one exception in that by far the most tightly bound complex involves a strong Si···N TB between SiF_4 and the lone pair of the thiazole N, with an interaction energy of 30 kcal mol^{-1}. Even accounting for its high deformation energy and entropic considerations, this structure remains as clearly the most stable at any temperature.

Received 5th January 2024,
Accepted 24th January 2024

DOI: 10.1039/d4cp00057a

rsc.li/pccp

Introduction

There are numerous Lewis acid–base interactions within the full constellation of noncovalent bonds. Probably the most well studied and understood of this class is the H-bond (HB) AH···B where the AH acid molecule accepts a certain amount of charge from the base B. In the most common such bond, it is a lone pair of B which transfers charge into the σ*(AH) antibonding orbital of the acid.[1–5] The HB is the prototype for a collection of similar bonds in which the bridging proton is replaced by other atoms, most of which are more electronegative than H. Many of these interactions are considered as closely related variants of the general σ-hole bond since they share a common feature consisting of a depletion of electron density along the extension of the R–A covalent bond, where A refers to the atom replacing H. Both this depletion and the resulting positive charge in the molecular electrostatic potential have been termed a σ-hole. Each such σ-hole bond is commonly categorized by the family of the A atom which contains this hole. The halogen atom X contains one such hole,[6–14] while a chalcogen Y atom would typically have two σ-holes,[15–27] one for each of its two R_2Y covalent bonds. This pattern continues with three σ-holes on the pnicogen Z atom of R_3Z,[28–35] and four for a tetrel atom T in a R_4T molecule.[21,36–43]

The growing accumulation of recent study has collectively developed a set of rules that govern the depth of the σ-hole and its resulting bond. This depth is heavily influenced by both the nature of the bridging A atom and any substituents R to which it is bonded. As one moves down a column of the periodic table, one typically sees a drop in the atom's electronegativity and a rise in polarizability. Both of these trends induce a deepening in the σ-hole and thereby a stronger bond with a base. Likewise, more powerful electron-withdrawing R substituents draw density away from A, aiding in the growth of this hole.

Of course, regions of positive potential are not necessarily limited to σ-holes that lie along these bond axes. It is not uncommon for positive potentials to occur directly above planar molecules.[44–58] For example, the F substituents on hexafluorobenzene extract density from the carbon ring which leaves the area above this ring with a positive potential. Likewise for a simpler molecule such as F_2CO where the positive region is situated above the C. These positive areas above planar molecules are commonly designated as π-holes, and like their σ-hole cousins, can engage in strong noncovalent bonding with a nucleophile.

The thiazole molecule presents a fascinating assortment of possibilities. Its five-membered heterocyclic ring contains both a N and S atom. A π-orbital of the N atom coalesces with the entire aromatic π-system that also contains two of the S atom's

[a] *Department of Chemistry and Biochemistry Utah State University Logan, Utah 84322-0300, USA. E-mail: steve.scheiner@usu.edu*
[b] *Department of Optics and Spectroscopy, Institute of Engineering Physics Samarkand State University 140104, University blv. 15, Samarkand, Uzbekistan*

electrons. In addition, the N and S atoms each contain a lone pair that lies in the plane of the ring. In combination with the region lying directly above the aromatic ring, there are thus a myriad of electron-rich regions in thiazole that could attract an electrophile. The four electron-withdrawing F substituents of CF_4 provide the C atom with four σ-holes, each of which have the capability to engage in a tetrel bond (TB) with a nucleophile, as has been demonstrated in the literature.[42,59,60] With its higher electropositivity and polarizability, the Si atom of the analogous SiF_4 ought to have deeper σ-holes on the central atom, and serve as a stronger partner in any such TB. Added to these options, each of the CH groups of thiazole can engage in a H-bond with any of the F atoms of the CF_4 or SiF_4.

The work described below is designed to explore the entire range of possibilities of bonding arrangements between thiazole and both CF_4 and SiF_4. The work thus addresses the competition between N and S, and between localized regions of charge buildup on a particular atom *versus* a more disperse area that lies over a larger aromatic ring. The thiazole unit can serve as electron donor or as acceptor, either within the context of a CH···F H-bond or in a chalcogen bond involving the S. The comparison between CF_4 and SiF_4 opens a window into the changes effected by moving down just one row in the periodic table with regard to tetrel bond strength with each of the aforementioned electron-rich regions. This inquiry is further motivated by a recent rotational spectroscopic analysis[61] that identified the most stable structure of the thiazole–CF_4 pair. However, the computational results suggested a number of alternative geometries, with very similar energetics, but failed to address the nature of the bonding within any of these structures despite their competitive nature.

Methods

Quantum chemical calculations were performed *via* the density functional approach (DFT), within the context of the M06-2X functional,[62] which has been shown to be an accurate means of treating noncovalent bonds of the sort of interest here.[63–73] An ultrafine grid was used for the M06-2X calculations, and a polarized triple-ζ def2-TZVP basis set[74] was chosen so as to afford a large and flexible set. Geometries were fully optimized and verified as true minima by the absence of imaginary vibrational frequencies. So as to ensure that all valid minima were identified, geometry optimizations were begun from forty different starting points with various attributes.

The Gaussian 16[75] program was chosen as the specific means to conduct these computations. The interaction energy E_{int} of each dyad was calculated as the difference between the energy of the complex and the sum of the energies of the two constituent subunits, each in the geometry they adopt within the dimer. The counterpoise procedure[76] was applied to correct basis set superposition error of E_{int}. Interaction energies were decomposed into individual components by the Symmetry Adapted Perturbation Theory (SAPT) approach[77] using the PSI4 program.[78] SAPT0 calculations employed the def2-TZVP basis set. The Multiwfn program[79] was applied to locate and quantify the extrema on the molecular electrostatic potential (MEP) of each monomer. Reduced density gradient diagrams were generated *via* the VMD program.[80] Atoms in Molecules (AIM) bond paths and their associated critical points[81] were located and their properties evaluated with the aid of the AIMAll program.[82] Interorbital charge transfers were monitored *via* the natural bond orbital (NBO) protocol[83] using the subroutines incorporated within Gaussian 16.

Results

The ELF diagram of thiazole in Fig. 1a clearly illustrates the lone pairs on both N and S that lie in the plane of the molecule. The molecular electrostatic potential (MEP) surrounding thiazole in Fig. 1b presents a roadmap of sorts as to where an electrophile might be attracted. The most negative region, as an extensive red area, lies near the N atom, both in the molecular plane and above it. The minimum in the MEP on a 0.001 a.u. isodensity surface is equal to −34.6 kcal mol^{-1}. There is a second, albeit not as strongly negative region, that lies directly above the C–C bond. This minimum is only −8.9 kcal mol^{-1}, but still negative enough to attract an electrophile. The area located above the S atom is slightly negative, as denoted by the yellow color, but not enough to actually contain a minimum. Both the CF_4 an SiF_4 molecules contain a classical σ-hole positive region directly along the extension of each F–T bond as witness the blue area in Fig. 1c and d. Due to its more electropositive character, the Si σ-hole is considerably deeper, with a maximum of 39.4 kcal mol^{-1}, as compared to only 19.4 kcal mol^{-1} for C. Judging only by the shapes of these MEPs, one might expect the blue σ-hole of TF_4 to be most strongly attracted to the N atom of thiazole, but also to the

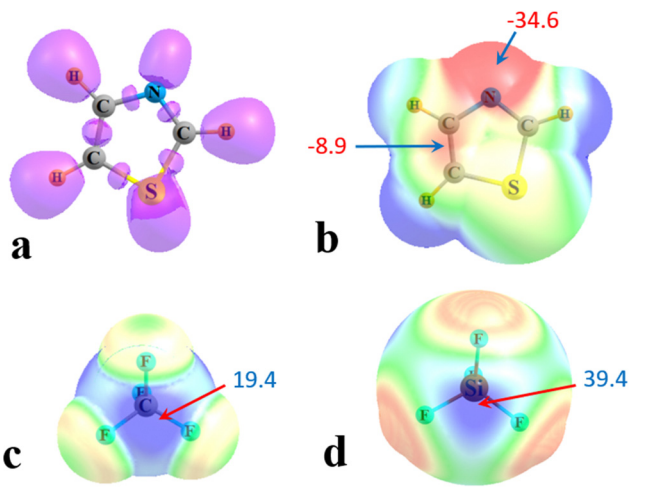

Fig. 1 (a) ELF diagram showing lone pairs on N and S of thiazole, contour shown is 0.8. Molecular electrostatic potential (MEP) surrounding (b) thiazole, (c) CF_4, (d) SiF_4 on surface corresponding to 1.5 × vdW radii. Blue and red colors respectively indicate positive and negative regions, with extrema of (a) +20, −10, (b) +10, 0, and (c) +13, −6 kcal mol^{-1}. Maximum (in blue) and minimum (in red) values displayed in kcal mol^{-1}.

π-region above the C–C bond albeit less so. The S atom is a possibility as well, but perhaps a dubious one due to the lack of a very negative MEP.

Dimer geometries and energetics

The thiazole molecule was combined first with CF_4 so as to ascertain all of the minima on the potential energy surface of this pair. Fig. 2 illustrates the six different minima that resulted from this extensive search. The Nπ geometry in Fig. 2a places the C atom of CF_4 above the N atom of thiazole, while the CF_4 lies in the molecular plane of Nσ, aligned with the N lone pair. There are two other geometries where the CF_4 is located above the plane of the ring. It lies nearly directly above the C–C bisector in the Cπ structure, and over the S in Sπ. In a fifth geometry type in Fig. 2e, one of the F atoms of CF_4 is positioned nearly along the extension of the C–S bond axis of thiazole, suggestive of a CS···F sort of chalcogen bond. There are three CH groups on thiazole, any of which can form a H-bond to a F atom. The one pictured in Fig. 2f utilizes the C_1H atom that lies between the N and S, but the geometries and other features of the two other H-bonded configurations are very similar.

Various aspects of the energetics of these structures are contained in Table 1. The first column lists the relative electronic energies which place the Nπ geometry as the most stable, followed closely by Nσ and Cπ, both of which lie within 0.2 kcal mol^{-1}. Slightly higher are Sπ and CS···F both still within 1 kcal mol^{-1} of Nπ. The H-bonded structures are a little higher in energy but still within 1.8 kcal mol^{-1}. The situation changes slightly when zero-point vibrational energies are added. As is evident in the next two columns of Table 1, the zero-point vibrational energies of the complexes are all in the range between 43.4 and 46.7 kcal mol^{-1}, with the CF_4 complexes a little higher in this regard. With either of the two TF_4 units, there are relatively small differences from one geometry to the next. The Nπ and Nσ dimers switch places with the latter now slightly lower in energy after inclusion of ZPVE. There is also a relative destabilization of Sπ up to 1.4 kcal mol^{-1}.

Table 1 Energetic parameters of various arrangements and interaction energies within dimers (kcal mol^{-1})

	E		ZPVE		E + ZPVE		G (298 K)		$-E_{int}$	
	C	Si	C	Si	C	Si	C	Si	C	Si
Nπ	0	—	46.66	—	0	—	0	—	1.78	—
Nσ	0.09	0	46.49	44.56	−0.09	0	−0.41	0	1.73	30.63
Cπ	0.19	6.71	46.66	43.83	0.19	5.97	0.10	4.42	1.62	3.11
Sπ	0.45	7.40	46.56	43.68	0.45	6.52	−0.46	4.25	1.35	2.42
CS···F	0.98	9.66	46.47	43.47	0.78	7.51	−1.20	4.62	0.90	1.32
C_1H···F	1.78	9.59	46.29	43.40	1.41	8.43	−0.77	2.33	0.24	0.49

Adding in entropic factors and setting a temperature of 298 K leads to the relative free energies G in the succeeding column. This inclusion reorders the energetics significantly. The chalcogen-bonded CS···F dimer becomes favored over the others, followed by the H-bonded geometry, and then Sπ and Nσ. Contrary to its favored status in terms of electronic energy, the Nπ structure becomes disfavored, lower in energy than only Cπ. The last energetic parameter listed in Table 1 is the interaction energy of each heterodimer. E_{int} is evaluated as the difference in energy between the complex and the sum of energies of the two monomers, each taking the internal geometry they adopt within the complex. The Nπ arrangement leads to the largest interaction energy of 1.78 kcal mol^{-1}. In fact the order of E_{int} parallels the purely electronic energies of the configurations, with the H-bonded dimer the most weakly bound.

A very recent study[61] had found that it is the Nσ structure that appears in the microwave spectrum of the thiazole–CF_4 pair. The rotational frequencies of this structure were measured to be 3.13, 0.43, and 0.40 GHz, in nice coincidence with our computed values of 3.14, 0.45, and 0.42 GHz. In addition to this geometry, calculations by these authors identified three other minima that correspond to our Nπ, Cπ, and one that would appear to roughly approximate our Sπ structure. The relative electronic energies of these three alternatives, including zero-point vibrational corrections, are 0.03, 0.10, and

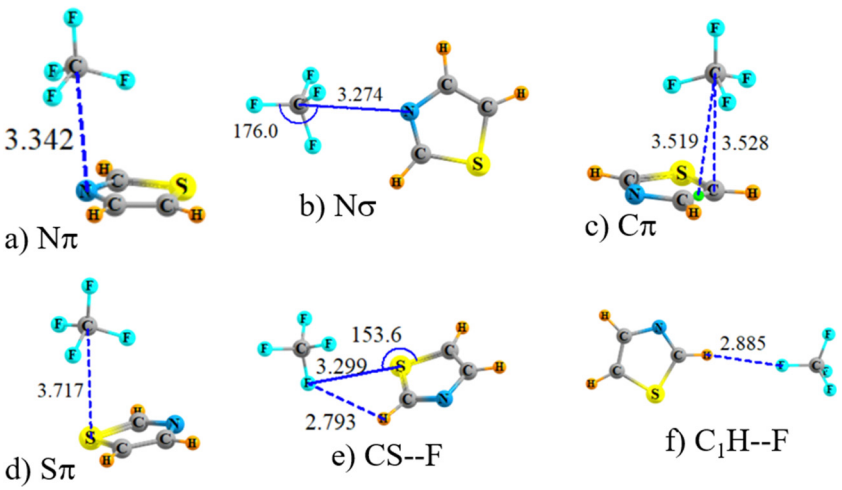

Fig. 2 Geometries of (a) Nπ, (b) Nσ, (c) Cπ, (d) Sπ, (e) CS--F, and (f) C_1H--F complexes between thiazole and CF_4. Distances in Å, angles in degs.

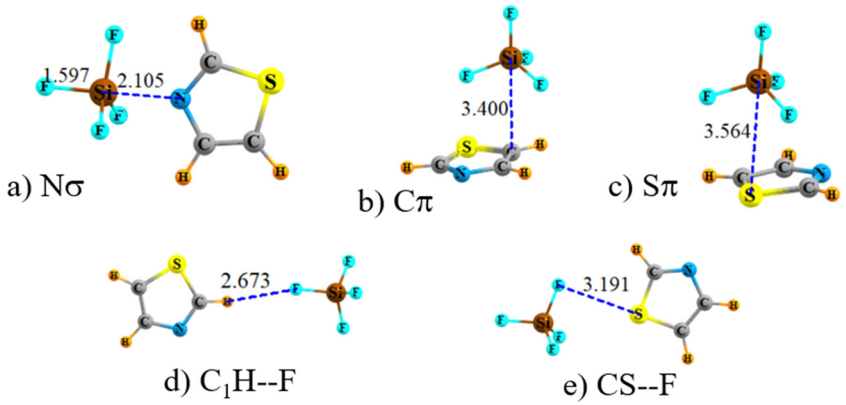

Fig. 3 Geometries of (a) Nσ, (b) Cπ, (c) Sπ, (d) C_1H--F, and (e) CS--F complexes between thiazole and SiF_4. Distances in Å, angles in degs.

0.20 kcal mol^{-1}, respectively, close to the values reported here in Table 1, with the exception of the Sπ dimer which is a bit higher in our calculations. Unlike our study, the calculations reported earlier did not include a CS$\cdots$F or any of the three H-bonded minima.

The replacement of the C of CF_4 by Si is expected to very substantially enhance the ability of this central atom to act as electron donor within the context of a tetrel bond. Search of the potential energy surface of the possible complexes of SiF_4 with thiazole led to the five geometries illustrated in Fig. 3. In keeping with the notion of a stronger tetrel bond, the R(Si$\cdots$N) distance in the Nσ configuration of Fig. 3a is only 2.105 Å, much shorter than the equivalent 3.274 Å in Fig. 2b. This noncovalent bond strengthening is obvious also in its interaction energy of 30.6 kcal mol^{-1}, listed in the last column of Table 1, far larger than the 1.7 kcal mol^{-1} of the CF_4 Nσ complex.

With regard to secondary minima, they are all much less stable than Nσ. The Cπ and Sπ geometries are about 7 kcal mol^{-1} higher in energy, and more than 4 kcal mol^{-1} higher than Nσ in terms of free energies. The H-bonded $C_1H\cdots F$ and CS$\cdots$F configurations are higher still, by nearly 10 kcal mol^{-1}, even though this difference is reduced to 2.3 kcal mol^{-1} when entropic considerations are added to the H-bonded structure. The Nπ geometry of CF_4 decays to Nσ during optimization.

The total entropy of each dimer is listed in Table 2, along with their rotational and vibrational components. The H-bonded structures in the last row have the largest entropy which leads to their stabilization relative to the others in terms of ΔG. Most of this enhanced entropy can be traced to their higher vibrational contributions. The entropy increases in an inverse relationship to the overall stability, *i.e.* Nσ < Cπ < Sπ < CS$\cdots$F < $C_1H\cdots$F, principally attributable to the vibrational entropy. It is for this reason that the stability ordering of ΔG is quite different than that of the energy.

Energy decomposition

The underlying nature of the bonding in these dimers can be assessed by partitioning each interaction energy into its components. SAPT decomposition yields first an electrostatic element (ES) resulting from the attraction between the nuclei and electron clouds of the two units, prior to any polarization caused by their mutual interaction. The stabilizing effects of this polarization and charge transfer fall under the heading of the induction (IND) component, complemented by dispersion energy (DISP). Pauli exchange (EX) resulting from the steric repulsions of the two molecular electron clouds prevent the two units from collapsing into one another.

The results of the SAPT partitioning listed in Table 3 indicate that the largest contributor to most of the interactions between thiazole and CF_4 originates in the dispersion energy. While ES is slightly larger than DISP for Nσ, it is the latter that is more important for the other structures, particularly for Sπ and CS$\cdots$F. Induction plays only a minor role in any of these dimers. The situation changes somewhat for the SiF_4 complexes. For the more loosely bound complexes in the last five rows of Table 4, ES is competitive with DISP, and even larger in several cases. But the most dramatic distinction is connected with the tightly bound Nσ structure, wherein all of the

Table 2 Total and contributions to entropy of complexes (cal mol^{-1} K^{-1})

	Total		Rotational		Vibrational	
	C	Si	C	Si	C	Si
Nπ	105.10	—	30.22	—	33.53	—
Nσ	104.75	100.72	30.65	30.39	32.75	28.71
Cπ	105.41	107.68	30.20	30.53	33.86	35.53
Sπ	108.10	110.45	30.22	30.53	36.53	38.30
CS$\cdots$F	112.36	111.20	30.52	30.99	40.49	38.59
$C_1H\cdots$F	122.50	124.30	31.81	32.16	49.34	50.52

Table 3 SAPT components of interaction energies (kcal mol^{-1}) in complexes pairing thiazole with CF_4

	ES	EX	IND	DISP	Total
Nσ	−2.95	3.65	−0.35	−2.29	−1.94
Nπ	−2.13	4.44	−0.25	−3.54	−1.48
Cπ	−2.19	4.79	−0.24	−3.55	−1.19
Sπ	−1.64	4.17	−0.21	−3.31	−0.99
CS$\cdots$F	−1.19	2.68	−0.18	−2.11	−0.80
$C_1H\cdots$F	−0.13	0.13	−0.02	−0.32	−0.34

Table 4 SAPT components of interaction energies (kcal mol^{-1}) in complexes pairing thiazole with SiF_4

	ES	EX	IND	DISP	Total
Nσ	−67.30	77.12	−21.20	−12.78	−24.16
Sπ	−3.22	6.57	−0.66	−4.08	−1.39
Cπ	−4.33	7.56	−0.73	−4.45	−1.96
CS···F	−1.72	3.29	−0.37	−2.19	−0.99
C_1H	−0.60	0.36	−0.07	−0.46	−0.78
C_2H	−0.56	0.39	−0.07	−0.50	−0.74

Table 5 Relative energetic parameters of various arrangements (kcal mol^{-1}) with different basis sets and GD3 dispersion correction

	M06-2X		M06-2X-GD3		M06-2X	
	Def2-TZVP		Def2-TZVP		6-311 + G**	
	C	Si	C	Si	C	Si
Nπ	0.00	—	0.00	—	0.00	—
Nσ	0.09	0	0.07	0.00	0.19	0.00
Cπ	0.19	6.71	0.19	6.70	0.23	10.21
Sπ	0.45	7.40	0.46	7.39	0.67	11.44
CS···F	0.98	9.66	0.99	8.60	1.50	13.12
C_1H···F	1.78	9.59	1.86	9.64	2.52	14.04

attractive components are magnified. Most notable, ES plays by far the largest role, followed by IND and then DISP.

It might be noted that SAPT predicts that the Nσ dyad of thiazole with CF_4 if a bit more stable than is Nπ, which reverses the supermolecule order in Table 1. This reversal is not attributable to the SAPT0 data in Table 3, since raising the level to SAPT2 maintains the same order, changing the total energies in the last column of Table 3 by less than 0.02 kcal mol^{-1}.

As another issue, some of the small energy differences encountered here between various dyads suggests the possibility that some relative energies might be reversed by alterations in the DFT functional or the basis set. Table 5 reaffirms a very low sensitivity to these issues. For example, the addition of a Grimme[84] D3 dispersion term has little to no effect upon the relative energies. The same insensitivity occurs if the basis set is changed from an Ahlrichs Def2-TZVP to a Pople-type 6-311+G**. Specifically, the latter set tends to enhance the stability of the preferred conformation relative to the secondary minima, but leaves the energetic ordering unchanged.

Electron density topology

Analysis of the electron density *via* AIM provides indications as to the specific bonding contacts between atoms. The AIM diagrams of the thiazole–CF_4 dimers in Fig. 4 provide some intriguing findings. Most notable, in no case is the central C atom of CF_4 implicated in a bonding interaction with the thiazole. It is the set of three F atoms that are tied to the thiazole N by bond paths for both Nπ and Nσ. The density of the bond critical point of these six bond paths in Fig. 4a and b are between 0.0052 and 0.0071 a.u., as summarized in Table 6, characteristic of a weak noncovalent bond. There are four separate bond paths in the Cπ dimer, which connect either to the C atoms of thiazole or to the C–C and C–S bonds. The S atom of thiazole is involved in only one of the three bond paths in the Sπ dimer, the other two leading to the neighboring C atoms. One of the two bond paths in CS···F is a direct product of the chalcogen bond, with the other indicating a CH···F H-bond. The rather weak CH···F H-bond in Fig. 4f is consistent with a low density of 0.0020 a.u. The AIM diagrams in Fig. 5 echo the failure of the central Si atom to be connected *via* a bond path to thiazole with one notable exception. The unambiguous presence of a Si···N tetrel bond in the Nσ conformer of Fig. 5a contains a large BCP density of 0.0573 a.u. The patterns within the other SiF_4 diagrams are similar to those of their CF_4 congeners, although the BCP densities are somewhat larger, mimicking the higher interaction energies of the former.

The BCP density of 0.0573 a.u. within the Nσ geometry of the SiF_4 complex falls within the usual limits of a noncovalent tetrel bond. The same categorization would result from the

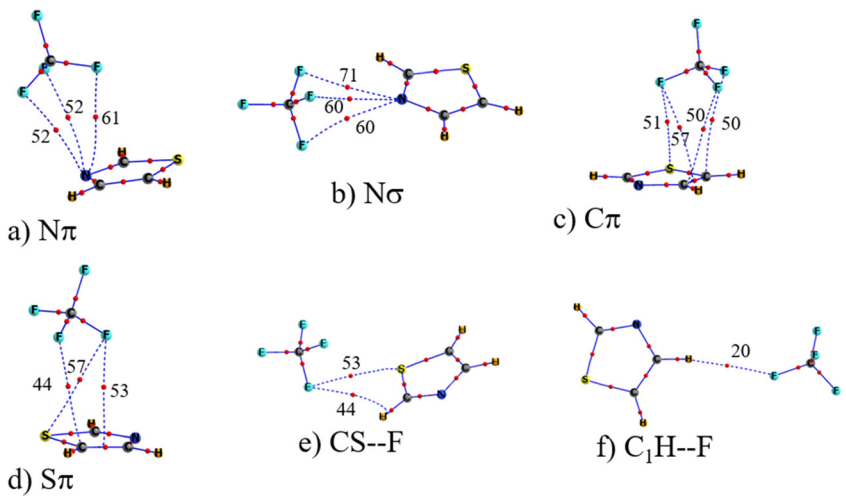

Fig. 4 AIM diagrams of complexes between (a) Nπ, (b) Nσ, (c) Cπ, (d) Sπ, (e) CS--F, and (f) C_1H--F thiazole and CF_4. Bond paths are indicated by broken lines with bond critical point shown by small red ball. Density at each BCP in 10^{-4} a.u.

Table 6 Bond critical point densities (10^{-4} a.u.), NBO E2 (kcal mol^{-1}), and total charge transferred CT to TF_4 (me)

	ρ_{BCP}		E2		CT	
	C	Si	C	Si	C	Si
Nπ	3 × 55	—	0.17	—	0.4	—
Nσ	3 × 67	573	0.12	23.04	−0.7	138.5
Cπ	3 × 52	3 × 69	0.32[a]	1.16[b]	0.7	2.0
Sπ	3 × 51	4 × 63	0.22	0.32	0.9	4.4
CS···F	2 × 49	73	0.33	0.51	0.0	0.6
C_1H···F	20	37	—	0.15	0.2	0.3

[a] π(CC)→σ*(CF) + F_{lp} → π. [b] π(CC)→σ*(SiF) + F_{lp} → π*(CC).

0.150 a.u. density Laplacian at this point. One can ascribe a small amount of covalency to this bond, based on its total energy density of −0.022 a.u. The formation of this complex induces a certain amount of distortion into the geometries of the two subunits. That of thiazole is minimal, amounting to only 0.5 kcal. However, the transition of SiF_4 from a perfect tetrahedron to something more akin to a trigonal bipyramid, with θ(FSiF) angles of 97°, causes an energy rise of 20.9 kcal mol^{-1}. It is for this reason that the energy difference between the Nσ configuration is only some 7–10 kcal mol^{-1} more stable than the other structures in Table 1, despite its very large interaction energy of 30.6 kcal mol^{-1}. The full reaction energy,[38,85–90] transforming a pair of optimized monomers to the Nσ complex would thus be exothermic with ΔE equal to −10 kcal mol^{-1}.

The reduced density gradient (RDG) offers a somewhat different graphical view of the bonding interactions. The intermolecular region in Fig. 6 takes on a blue color for strongly attractive regions, green for mildly attractive, and turns red for repulsions. The colored area of Fig. 6a for the Nσ conformer of CF_4 is rather diffuse, covering not only the central C but also the three neighboring F atoms. In addition, the green color is deeper in hue along the N···F lines, all conforming to the AIM diagram of Fig. 4a. Replacing CF_4 by SiF_4 within this same Nσ geometry provides a very different picture in Fig. 6b. The Si···N region is very blue, fading to repulsive red as one moves away from the central Si and toward the peripheral F centers. This pattern strongly supports the AIM Si···N bond path and a tetrel bond. The Nπ configuration of CF_4 in Fig. 6c is not unlike that for its Nσ geometry in Fig. 6a, also in line with the AIM picture of three separate N···F bond paths in Fig. 4b.

Electronic displacements

NBO treatment is frequently very helpful in elucidating the particular atoms involved in molecular interactions as well as the relevant orbitals on each, offering an alternate view to AIM. However there are certain discrepancies between these two different views of bonding. Taking the Nσ interaction with CF_4 as an example, the NBO data in Table 6 suggest the presence of a C···N tetrel bond with a E2 perturbation energy of 0.12 kcal mol^{-1} for N_{lp} → σ*(CF), although no such bond was suggested by AIM. The three AIM F···N bond paths in Fig. 4a, each to a different F atom, are reduced to the involvement of only one of these F centers, with charge transfers from the F lone pair to three different π MOs of the thiazole. A similar discrepancy arises in the Nπ configuration. NBO again suggests the involvement of only one of the F atoms of CF_4, where its lone pair transfers density to two different thiazole MOs. NBO is less ambiguous and consistent with AIM in its finding of a Si···N tetrel bond in the Nσ dimer with SiF_4. The E2 perturbation for charge transfer from NC bonding orbitals of thiazole to the appropriate σ*(SiF) antibonding orbital is 23.0 kcal mol^{-1}, supplemented by 13 kcal mol^{-1} transfers to each of the other three SiF σ* orbitals.

The fundamental distinctions between the Nσ dimers involving C and Si are highlighted by electron density shift diagrams which are derived when the electron densities of the two monomers are subtracted from that of the full complex. The purple and green regions of Fig. 7 show respectively gain and loss of density as a result of the dimerization process. The pattern in Fig. 7b for SiF_4 is characteristic of a tetrel bond, with a large purple density enhancement in the region between the Si and N nuclei, and a small depletion closer to the N. The pattern is quite different for the CF_4 analog in Fig. 7a where the

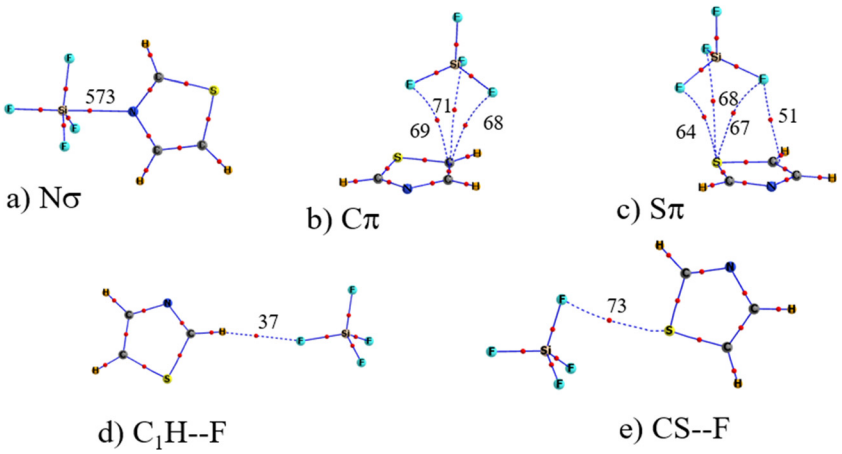

Fig. 5 AIM diagrams of (a) Nσ, (b) Cπ, (c) Sπ, (d) C_1H--F, and (e) CS--F complexes between thiazole and SiF_4. Bond paths are indicated by broken lines with bond critical point shown by small red ball. Density at each BCP in 10^{-4} a.u.

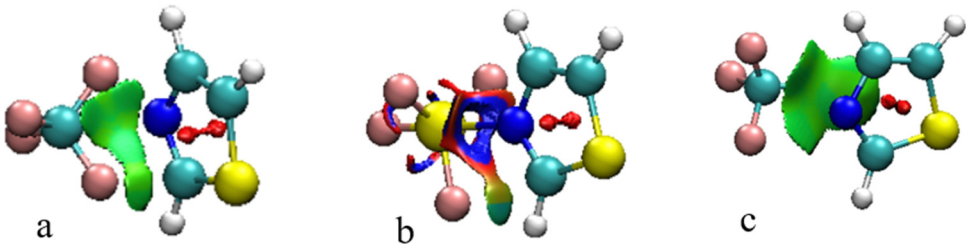

Fig. 6 RDG diagrams of Nσ complexes of thiazole with (a) CF_4 and (b) SiF_4; (c) Nπ geometry of CF_4. Contour shown has RDG = 0.5 a.u., with blue and red color extremes representing (sign λ_2) ρ = −0.03 and +0.03 a.u., respectively.

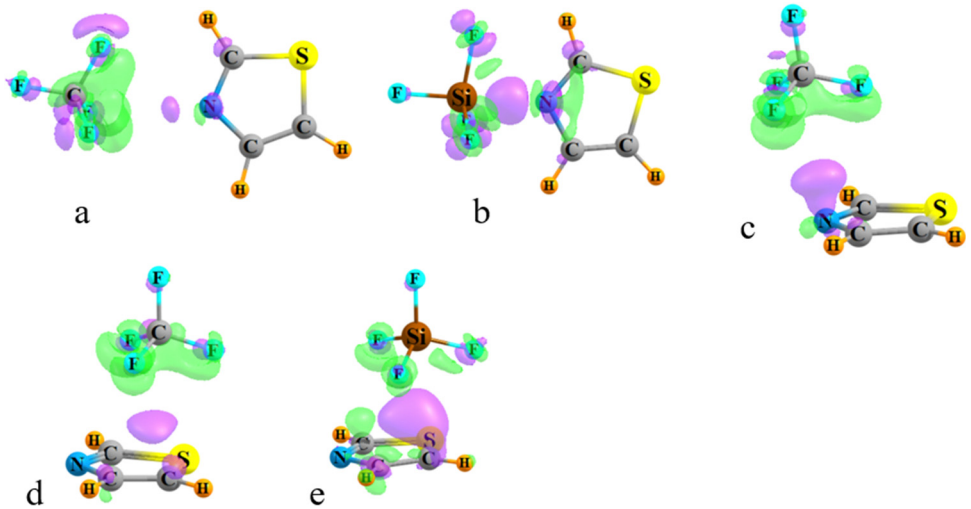

Fig. 7 Electron density shifts accompanying formation of complexes of thiazole with (a) CF_4 in Nσ structure, (b) SiF_4 in Nσ structure, (c) CF_4 in Nπ structure, (d) CF_4 in Cπ structure, (e) SiF_4 in Cπ structure. Purple and green colors respectively indicate gain and depletion of density, with contours shown (a) ±0.0005, (b) ±0.005, (c) ±0.0004, (d) ±0.0003, (e) ±0.0005 a.u.

dominant feature between the C and N nuclei is a substantial green depletion. As an illustration of the density shifts in the π-type complexes, one sees a loss near the F nuclei of CF_4 in the Nπ complex in Fig. 7c, with an accretion in the region lying above the N. The EDS diagrams of the Cπ arrangements of the CF_4 and SiF_4 complexes are exhibited in Fig. 7d and e. These patterns are similar to that in Fig. 7c which are characterized by a gain above the C atom of the thiazole, and depletions on the three F atoms of TF_4.

As a quantitative measure of overall density motions from one molecule to the other, the total charge transfer (CT) in the last columns of Table 6 was computed as the sum of the natural charges of all the atoms on each monomer. In line with the weak interactions within the CF_4 complexes, the total charge transferred from thiazole to CF_4 are all less than 1 me. These quantities are much larger for SiF_4, with CT equal to 2 and 4 me, respectively, for the Cπ and Sπ geometries. But by far the largest transfer occurs within the Nσ structure, with 139 me moving from thiazole to SiF_4, another indicator of a true tetrel bond.

Internal deformations

Since most of these interactions are fairly weak, one would not anticipate that the internal geometries of the two monomers would be much affected by the complexation. The bondlength changes within the two subunits are reported in Tables 7 and 8 for the dyads containing CF_4 and SiF_4, respectively. As indicated by the first row of Table 7, the approach of the CF_4 unit above

Table 7 Changes in internal bondlengths (Å) caused by complexation of thiazole with CF_4

	$N–C_1$	$C_1–S$	$S–C_2$	$C_2–C_3$	$C_3–N$	$C–F_1$	$C–F_2$
Nπ	0.0007	−0.0014	−0.0004	0.0000	0.0002	0.0034	−0.0019
Nσ	0.0005	−0.0016	0.0000	−0.0001	0.0000	0.0060	0.0024
Cπ	0.0000	−0.0002	−0.0001	0.0005	−0.0001	0.0012	0.0019
Sπ	−0.0004	0.0000	−0.0002	0.0000	0.0005	0.0010	0.0015
CS···F	−0.0005	0.0010	0.0002	−0.0002	0.0004	−0.0008	−0.0014
C_1H···F	0.0001	−0.0007	−0.0006	0.0003	0.0001	0.0029	−0.0013

Table 8 Changes in internal bondlengths (Å) caused by complexation of thiazole with SiF_4

	$N–C_1$	$C_1–S$	$S–C_2$	$C_2–C_3$	$C_3–N$	$Si–F_1$	$Si–F_2$
Nσ	0.0085	−0.0214	0.0022	−0.0055	0.0021	0.0394	0.0342
Cπ	−0.0002	−0.0004	0.0008	0.0017	−0.0003	0.0022	0.0025
Sπ	−0.0016	0.0036	0.0016	−0.0009	0.0010	0.0017	0.0024
CS···F	−0.0008	−0.0005	−0.0008	0.0000	0.0008	−0.0001	0.0029
C_1H···F	0.0002	0.0001	−0.0001	0.0000	0.0002	0.0025	−0.0015

the thiazole N atom in the Nπ structure induces a slight elongation of the two bonds to the N, with small contractions of the other bonds. In keeping with the charge transfer to the CF_1 antibonding orbital, this bond stretches a bit. Fairly similar changes are noted in the Nσ structure. As the CF_4 approaches the $C_2–C_3$ midpoint in the Cπ geometry, this bond lengthens, whereas the thiazole bondlengths are relatively unaffected by the Sπ complexation. The largest change occurring within the CS···F structure is the lengthening of the $C_1–S$ bond, attributable to the transfer into the corresponding σ* antibonding orbital.

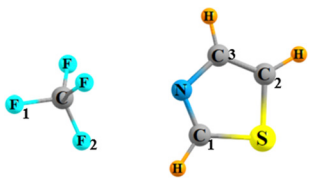

For the most part, the bondlength changes when thiazole is complexed with SiF_4 in Table 8 mirror those in Table 7 with some exceptions. In the first place, given the somewhat stronger bonding with SiF_4 as compared to CF_4, a number of changes are larger in Table 8. For example, the two bonds connecting to S barely change in the Sπ geometry with CF_4, whereas elongations of 0.004 and 0.002 Å occur with SiF_4. But the most dramatic distinction is associated with the Nσ configuration. The order of magnitude increase in the interaction energy for SiF_4 is reflected in quite substantial bondlength changes. The two bonds to N are stretched by 0.002 and 0.009 Å, accompanied by a substantial contraction of the $C_1–S$ bond. Also all four of the Si–F bonds undergo a stretch of 0.034 to 0.039 Å, due in large measure to the additional density added to their σ*(SiF) antibonding orbitals.

Conclusions

There exists a delicate balance between the various geometries of the heterodimer involving thiazole and CF_4. All of the structures are weakly bound with interaction energies less than 2 kcal mol^{-1}. The two most stable conformers orient the CF_4 near the thiazole N atom, either in the molecular plane or directly above the N. Two other configurations, only slightly less stable, place the CF_4 above either the thiazole C–C bond or its S atom. There is also a chalcogen-bonded CS···F configuration, as well as H-bonded complexes to each of the CH groups of thiazole. The energetic ordering of these various structures is scrambled when entropic considerations are included in their free energies, making the chalcogen-bonded geometry most stable. The replacement of the C of CF_4 by Si leads to an unambiguous identification of a structure with SiF_4 located within the thiazole plane as by far the most stable. This Si···N tetrel-bonded heterodimer has an interaction energy of 30.6 kcal mol^{-1}. The Cπ, Sπ, and CS···F geometries remain as minima, more tightly bound than their analogues with CF_4, but still far less stable than the global minimum. Despite the lone pair on S, this region is unable to attract either electrophile.

The global thiazole–SiF_4 minimum clearly involves a tetrel bond with a high proportion of electrostatic stabilization. However, the other minima identified on the two potential energy surfaces contain much higher proportions of dispersion, in most cases even larger than the electrostatic component; induction contributions are minimal. The tetrel-bonded thiazole–SiF_4 heterodimer is the only species for which there is an AIM bond path that involves the central tetrel atom. The bond paths of most of the other configurations connect the F atoms of TF_4 to the thiazole. This lack of direct central T atom involvement in the bonding is largely verified by NBO and RDG analyses, as well as mappings of the electron density shift patterns. Overall, this work reinforces the reluctance of the C atom to engage in tetrel bonds, in strong contrast to its heavier congeners such as Si.

There are several lessons to be gleaned from the calculations presented here. Firstly, they demonstrate how a molecule like thiazole, with a few electrophilic sites, is able to bind to a simple molecule like CF_4 in a number of entirely different ways. A tetrel bond can be formed between the C of CF_4 to the N, both to its lone pair in the molecular plane, and directly above the N. With CF_4 hovering above the thiazole plane, the tetrel bond can also engage with the S atom and with a C=C π-bond. Some of these dyads occur despite the absence of a corresponding minimum in the MEP of the thiazole, so the presence of such a minimum is clearly not a prerequisite for the formation of a stable structure. There is also the possibility of an interaction that involves an entirely distinct CS···F chalcogen bond when one F of CF_4 lies in the thiazole plane; all of these various configurations are complemented by three different CH···F H-bonded structures. One of the remarkable features of this molecular pairing is the tight clustering of the energies of these eight different structures, all within 2 kcal mol^{-1} of one another. Despite their similar energies, these complexes are bound together by diverse interactions, *viz.* tetrel, chalcogen, and hydrogen bonds. Another important lesson is the way in which the energy ordering changes upon addition of zero-point

vibrations, which is further remodified when entropic factors are included. The expectations as to the structure to be expected in an experiment are thus heavily dependent upon the particular temperature.

A second important conclusion is connected with the modification that arises when the C of CF_4 is replaced by its Si congener. While most of the configurations observed for CF_4 remain intact, there is a larger spread of their relative energies. Nonetheless, the energy ordering is again modified by the inclusion of entropic effects which make the H-bonded structures preferred at higher temperatures, despite their higher electronic energy. But the principal difference incurred by this C → Si substitution is the prominence of the planar Si···N tetrel-bonded structure which is some 30 times stronger than its C···N analogue, with an interaction energy of 30.6 kcal mol^{-1}. It is this structure which is inarguably the one that will be observed experimentally, regardless of temperature. The enormous enhancement in the interaction energy within this Si···N tetrel bond can be attributed in part to the deeper σ-hole on Si. But it should be noted that the amplifications of the several other interactions in the SiF_4···triazole pair are much milder, despite their interaction with this same σ-hole.

With regard to the various computational tools applied to this series of complexes, the calculation of the electronic energy does not fully conform to the result obtained if corrected by zero-point vibrational energies; the energetic ordering is further adjusted when entropic effects are added. The SAPT formulation provides interaction energies in good accord with the supermolecule approach when corrected for basis set superposition error. It is also worth noting that the addition of a further dispersion term to the DFT functional has little effect upon relative energetics, nor does application of a different sort of triple-valence basis set. In terms of various quantities that are derived from the wavefunctions, the AIM bond paths provide evidence as to the particular atoms of the two units that are bonded to one another, so help to distinguish between say, a tetrel bond and a set of F···N interactions. However, AIM tends toward atom–atom bonding, even in π-systems where the interaction might be better described as connecting to a bond midpoint. Pictorial RDG patterns tend to favor a rather diffuse sort of bonding in many cases, clouding a more specific bonding picture; the same is true for some electron density shift maps. It is worth noting that NBO bonding pictures are not always consistent with AIM.

Author contributions

Conceptualization SS; data curation AA; formal analysis SS; funding acquisition SS; writing SS and AA; visualization AA; supervision SS; investigation AA.

Conflicts of interest

The authors declare no conflict of interest.

Acknowledgements

This material is based upon work supported by the National Science Foundation under Grant No. 1954310.

References

1 G. C. Pimentel and A. L. McClellan, *The Hydrogen Bond*, Freeman, San Francisco, 1960.
2 M. D. Joesten and L. J. Schaad, *Hydrogen Bonding*, Marcel Dekker, New York, 1974.
3 G. R. Desiraju and T. Steiner, *The Weak Hydrogen Bond in Structural Chemistry and Biology*, Oxford, New York, 1999.
4 G. A. Jeffrey and W. Saenger, *Hydrogen Bonding in Biological Structures*, Springer-Verlag, Berlin, 1991.
5 G. Gilli and P. Gilli, *The Nature of the Hydrogen Bond*, Oxford University Press, Oxford, UK, 2009.
6 D. F. Mertsalov, R. M. Gomila, V. P. Zaytsev, M. S. Grigoriev, E. V. Nikitina, F. I. Zubkov and A. Frontera, *Crystal*, 2021, **11**, 1406.
7 J. E. Del Bene, I. Alkorta and J. Elguero, *Chem. Phys. Lett.*, 2020, **761**, 137916.
8 M. Palusiak and S. J. Grabowski, *Struct. Chem.*, 2008, **19**, 5–11.
9 S. J. Grabowski, *J. Phys. Chem. A*, 2011, **115**, 12340–12347.
10 S. Scheiner and S. Hunter, *Chem. Phys. Chem.*, 2022, **23**, e202200011.
11 J. S. Murray and P. Politzer, *Chem. Phys. Chem.*, 2021, **22**, 1201–1207.
12 A. Amonov and S. Scheiner, *Molecules*, 2023, **28**, 7520.
13 G. Cavallo, P. Metrangolo, R. Milani, T. Pilati, A. Priimagi, G. Resnati and G. Terraneo, *Chem. Rev.*, 2016, **116**, 2478–2601.
14 S. Scheiner, *CrystEngComm*, 2013, **15**, 3119–3124.
15 G. R. Desiraju and V. Nalini, *J. Mater. Chem.*, 1991, **1**, 201–203.
16 M. Iwaoka and S. Tomoda, *J. Am. Chem. Soc.*, 1994, **116**, 2557–2561.
17 R. J. Fick, G. M. Kroner, B. Nepal, R. Magnani, S. Horowitz, R. L. Houtz, S. Scheiner and R. C. Trievel, *ACS Chem. Biol.*, 2016, **11**, 748–754.
18 A. J. Mukherjee, S. S. Zade, H. B. Singh and R. B. Sunoj, *Chem. Rev.*, 2010, **110**, 4357–4416.
19 L. M. Azofra and S. Scheiner, *J. Chem. Phys.*, 2015, **142**, 034307.
20 J. Fanfrlík, A. Přáda, Z. Padělková, A. Pecina, J. Macháček, M. Lepšík, J. Holub, A. Růžička, D. Hnyk and P. Hobza, *Angew. Chem., Int. Ed.*, 2014, **53**, 10139–10142.
21 A. C. Legon, *Phys. Chem. Chem. Phys.*, 2017, **19**, 14884–14896.
22 C. Trujillo, I. Rozas, J. Elguero, I. Alkorta and G. Sánchez-Sanz, *Phys. Chem. Chem. Phys.*, 2019, **21**, 23645–23650.
23 S. Scheiner and J. Lu, *Chem. – Eur. J.*, 2018, **24**, 8167–8177.
24 O. Carugo, G. Resnati and P. Metrangolo, *ACS Chem. Biol.*, 2021, **16**, 1622–1627.
25 S. Scheiner, *CrystEngComm*, 2021, **23**, 6821–6837.

26 H. S. Biswal, A. K. Sahu, B. Galmés, A. Frontera and D. Chopra, *ChemBioChem*, 2022, **23**, e202100498.
27 K. T. Mahmudov, A. V. Gurbanov, V. A. Aliyeva, M. F. C. Guedes da Silva, G. Resnati and A. J. L. Pombeiro, *Coord. Chem. Rev.*, 2022, **464**, 214556.
28 J. E. Del Bene, I. Alkorta, G. Sanchez-Sanz and J. Elguero, *J. Phys. Chem. A*, 2011, **115**, 13724–13731.
29 A. Amonov and S. Scheiner, *Phys. Chem. Chem. Phys.*, 2023, **25**, 23530–23537.
30 A. Bauzá, D. Quiñonero, P. M. Deyà and A. Frontera, *Phys. Chem. Chem. Phys.*, 2012, **14**, 14061–14066.
31 Q.-Z. Li, R. Li, X.-F. Liu, W.-Z. Li and J.-B. Cheng, *Chem. Phys. Chem.*, 2012, **13**, 1205–1212.
32 G. Sánchez-Sanz, I. Alkorta, C. Trujillo and J. Elguero, *Chem. Phys. Chem.*, 2013, **14**, 1656–1665.
33 D. Setiawan, E. Kraka and D. Cremer, *J. Phys. Chem. A*, 2015, **119**, 1642–1656.
34 Z. Latajka and S. Scheiner, *J. Chem. Phys.*, 1986, **84**, 341–347.
35 U. Adhikari and S. Scheiner, *Chem. Phys. Lett.*, 2012, **536**, 30–33.
36 D. Mani and E. Arunan, *J. Phys. Chem. A*, 2014, **118**, 10081–10089.
37 P. R. Varadwaj, A. Varadwaj, H. M. Marques and K. Yamashita, *CrystEngComm*, 2023, **25**, 1411–1423.
38 S. Scheiner, *Phys. Chem. Chem. Phys.*, 2021, **23**, 5702–5717.
39 V. d P. N. Nziko and S. Scheiner, *Phys. Chem. Chem. Phys.*, 2016, **18**, 3581–3590.
40 S. J. Grabowski, *Crystal*, 2022, **12**, 112.
41 A. Grabarz, M. Michalczyk, W. Zierkiewicz and S. Scheiner, *Chem. Phys. Chem.*, 2020, **21**, 1934–1944.
42 W. Zierkiewicz, M. Michalczyk, R. Wysokiński and S. Scheiner, *Molecules*, 2019, **24**, 376.
43 C. Trujillo, I. Alkorta, J. Elguero and G. Sánchez-Sanz, *Molecules*, 2019, **24**, 308.
44 A. Ruigrok van der Werve, Y. R. van Dijk and T. J. Mooibroek, *Chem. Commun.*, 2018, **54**, 10742–10745.
45 W. Zierkiewicz, M. Michalczyk and S. Scheiner, *Phys. Chem. Chem. Phys.*, 2018, **20**, 4676–4687.
46 S. J. Grabowski, *Phys. Chem. Chem. Phys.*, 2017, **19**, 29742–29759.
47 A. Bauzá and A. Frontera, *Coord. Chem. Rev.*, 2020, **404**, 213112.
48 V. d P. N. Nziko and S. Scheiner, *Phys. Chem. Chem. Phys.*, 2016, **18**, 3581–3590.
49 A. Bauza and A. Frontera, *Phys. Chem. Chem. Phys.*, 2015, **17**, 24748–24753.
50 J. E. Del Bene, I. Alkorta and J. Elguero, *J. Phys. Chem. A*, 2013, **117**, 11592–11604.
51 M. Solimannejad, V. Ramezani, C. Trujillo, I. Alkorta, G. Sánchez-Sanz and J. Elguero, *J. Phys. Chem. A*, 2012, **116**, 5199–5206.
52 J. S. Murray, P. Lane, T. Clark, K. E. Riley and P. Politzer, *J. Mol. Model.*, 2012, **18**, 541–548.
53 W. Zierkiewicz, M. Michalczyk and S. Scheiner, *Molecules*, 2021, **26**, 1740.
54 M. Hou, Z. Liu and Q. Li, *Int. J. Quantum Chem.*, 2020, **120**, e26251.
55 J. Echeverría, *CrystEngComm*, 2017, **19**, 6289–6296.
56 A. Bauzá, A. Frontera and T. J. Mooibroek, *Chem. – Eur. J.*, 2019, **25**, 13436–13443.
57 W. Dong, B. Niu, S. Liu, J. Cheng, S. Liu and Q. Li, *Chem. Phys. Chem.*, 2019, **20**, 627–635.
58 S. Scheiner, *J. Phys. Chem. A*, 2021, **125**, 6514–6528.
59 S. Scheiner, *J. Phys. Chem. A*, 2017, **121**, 5561–5568.
60 M. Michalczyk, W. Zierkiewicz, R. Wysokiński and S. Scheiner, *Chem. Phys. Chem.*, 2019, **20**, 959–966.
61 T. Yang, Y. Xu, Z. Wang, C. Feng and G. Feng, *Phys. Chem. Chem. Phys.*, 2023, **25**, 25566–25572.
62 Y. Zhao and D. G. Truhlar, *Theor. Chem. Acc.*, 2008, **120**, 215–241.
63 K. Kříž and J. Řezáč, *Phys. Chem. Chem. Phys.*, 2022, **24**, 14794–14804.
64 A. D. Boese, *ChemPhysChem*, 2015, **16**, 978–985.
65 S. Kozuch and J. M. L. Martin, *J. Chem. Theory Comput.*, 2013, **9**, 1918–1931.
66 M. Walker, A. J. A. Harvey, A. Sen and C. E. H. Dessent, *J. Phys. Chem. A*, 2013, **117**, 12590–12600.
67 K. S. Thanthiriwatte, E. G. Hohenstein, L. A. Burns and C. D. Sherrill, *J. Chem. Theory Comput.*, 2011, **7**, 88–96.
68 M. S. Liao, Y. Lu and S. Scheiner, *J. Comput. Chem.*, 2003, **24**, 623–631.
69 M. J. Deible, O. Tuguldur and K. D. Jordan, *J. Phys. Chem. B*, 2014, **118**, 8257–8263.
70 A. Li, H. S. Muddana and M. K. Gilson, *J. Chem. Theory Comput.*, 2014, **10**, 1563–1575.
71 N. Mardirossian and M. Head-Gordon, *J. Chem. Theory Comput.*, 2013, **9**, 4453–4461.
72 J. Elm, M. Bildeb and K. V. Mikkelsena, *Phys. Chem. Chem. Phys.*, 2013, **15**, 16442–16445.
73 S. Bhattacharyya, A. Bhattacherjee, P. R. Shirhatti and S. Wategaonkar, *J. Phys. Chem. A*, 2013, **117**, 8238–8250.
74 F. Weigend and R. Ahlrichs, *Phys. Chem. Chem. Phys.*, 2005, **7**, 3297–3305.
75 M. J. Frisch, G. W. Trucks, H. B. Schlegel, G. E. Scuseria, M. A. Robb, J. R. Cheeseman, G. Scalmani, V. Barone, G. A. Petersson, H. Nakatsuji, X. Li, M. Caricato, A. V. Marenich, J. Bloino, B. G. Janesko, R. Gomperts, B. Mennucci, H. P. Hratchian, J. V. Ortiz, A. F. Izmaylov, J. L. Sonnenberg, D. Williams-Young, F. Ding, F. Lipparini, F. Egidi, J. Goings, B. Peng, A. Petrone, T. Henderson, D. Ranasinghe, V. G. Zakrzewski, J. Gao, N. Rega, G. Zheng, W. Liang, M. Hada, M. Ehara, K. Toyota, R. Fukuda, J. Hasegawa, M. Ishida, T. Nakajima, Y. Honda, O. Kitao, H. Nakai, T. Vreven, K. Throssell, J. A. Montgomery Jr., J. E. Peralta, F. Ogliaro, M. J. Bearpark, J. J. Heyd, E. N. Brothers, K. N. Kudin, V. N. Staroverov, T. A. Keith, R. Kobayashi, J. Normand, K. Raghavachari, A. P. Rendell, J. C. Burant, S. S. Iyengar, J. Tomasi, M. Cossi, J. M. Millam, M. Klene, C. Adamo, R. Cammi, J. W. Ochterski, R. L. Martin, K. Morokuma, O. Farkas, J. B. Foresman and D. J. Fox, *Gaussian 16*, Wallingford, 2016.
76 S. F. Boys and F. Bernardi, *Mol. Phys.*, 1970, **19**, 553–566.

77 K. Szalewicz and B. Jeziorski, in *Molecular Interactions. From van der Waals to Strongly Bound Complexes*, ed. S. Scheiner, Wiley, New York, 1997, pp. 3–43.
78 D. G. A. Smith, L. A. Burns, A. C. Simmonett, R. M. Parrish, M. C. Schieber, R. Galvelis, P. Kraus, H. Kruse, R. D. Remigio, A. Alenaizan, A. M. James, S. Lehtola, J. P. Misiewicz, M. Scheurer, R. A. Shaw, J. B. Schriber, Y. Xie, Z. L. Glick, D. A. Sirianni, J. S. O'Brien, J. M. Waldrop, A. Kumar, E. G. Hohenstein, B. P. Pritchard, B. R. Brooks, H. F. SchaeferIII, A. Y. Sokolov, K. Patkowski, A. E. DePrinceIII, U. Bozkaya, R. A. King, F. A. Evangelista, J. M. Turney, T. D. Crawford and C. D. Sherrill, *J. Chem. Phys.*, 2020, **152**, 184108.
79 T. Lu and F. Chen, *J. Comput. Chem.*, 2012, **33**, 580–592.
80 W. Humphrey, A. Dalke and K. Schulten, *J. Mol. Graphics*, 1996, **14**, 33–38.
81 R. F. W. Bader, *Atoms in Molecules, A Quantum Theory*, Clarendon Press, Oxford, 1990.
82 T. A. Keith and T. K. Gristmill, *Software*, Overland Park KS, 2013.
83 A. E. Reed, F. Weinhold, L. A. Curtiss and D. J. Pochatko, *J. Chem. Phys.*, 1986, **84**, 5687–5705.
84 S. Grimme, J. Antony, S. Ehrlich and H. Krieg, *J. Chem. Phys.*, 2010, **132**, 154104.
85 K. Szalewicz and B. Jeziorski, *J. Chem. Phys.*, 1998, **109**, 1198–1200.
86 R. Kalescky, E. Kraka and D. Cremer, *J. Chem. Phys.*, 2014, 140.
87 R. A. Shaw, J. G. Hill and A. C. Legon, *J. Phys. Chem. A*, 2016, **120**, 8461–8468.
88 R. Wysokiński, M. Michalczyk, W. Zierkiewicz and S. Scheiner, *Phys. Chem. Chem. Phys.*, 2019, **21**, 10336–10346.
89 W. Zierkiewicz, M. Michalczyk and S. Scheiner, *Phys. Chem. Chem. Phys.*, 2018, **20**, 8832–8841.
90 S. Scheiner, *J. Phys. Chem. A*, 2018, **122**, 2550–2562.